Journal of Visualization, Vol. 6, No. 4 (2003) 407-416

Liquid Crystal Heat Transfer Measurements in a Rectangular Channel with Solid and Slit Rib

Panigrahi, P. K.* and Tariq, A.*

* Mechanical Engineering Department, IIT Kanpur, U.P. 208016, India.
E-mail: panig@iitk.ac.in ; atariq@iitk.ac.in

Received 5 August 2002.
Revised 6 March 2003.

Abstract : An experimental investigation on the heat transfer effectiveness of solid and slit ribs mounted on the bottom surface of a rectangular channel has been carried out at Reynolds numbers of 13400, 22600, 32100 and 40800. The rib height to hydraulic diameter ratio (e/D_h) set during experiment is equal to 0.0624. The surface Nusselt number results from transient liquid crystal thermography are presented. The heat transfer enhancement performance analysis has been carried out using entropy generation principle. The slit rib is superior to solid rib from both heat transfer augmentation and pressure penalty point of view. The performance of the slit rib is a function of the open area ratio (β) and the location of the slit (b) from the bottom test surface. The optimum open area ratio is 20% and the slit located symmetrically from the top and bottom surface of the rib is the optimum location of the slit. The heat transfer augmentation of the slit rib (β = 20%) is 61% in comparison to 40% for the solid rib at Re = 32100 and the pressure penalty for the slit rib is 7% lower than the solid rib. The entropy generation for the slit rib is 33% less than that of the solid rib.

Keywords : Heat transfer enhancement, Solid rib, Slit rib, Entropy generation, Liquid crystal thermography.

1. Introduction

Rib turbulators are used to improve the convective heat transfer coefficient in many practical applications i.e. gas turbine blade cooling passages, heat exchanger surfaces, gas-cooled reactor fuel elements and ventilation equipment of micro-electronic systems. Han and Zhang (1992) investigated the effect of broken rib orientations on the local heat transfer distributions and pressure drop in a square channel and showed that the 60° V-shaped broken rib gives higher heat transfer augmentation than other broken rib configurations while the 90° broken rib produces the largest pressure drop. Acharya et al. (1993) presented the average Nusselt number and overall pressure drop in a ribbed duct with vortex generators (circular rods) placed immediately above or just downstream of select rib elements and observed that best performance is obtained when placing the largest diameter vortex generator directly over every rib. Kukreja et al. (1993) studied the turbulent heat/mass transfer characteristics by the naphthalene sublimation technique in a square channel with arrays of full ribs and V-shaped ribs and observed that secondary flows caused by oblique ribs interact with the main flow and affect the flow reattachment and recirculation between the ribs and interrupt the boundary layer growth downstream of the reattachment regions. Chyu and Natarajan (1993) investigated the heat transfer of inline-slit ribs and staggered-slit ribs mounted on the bottom

wall using naphthalene sublimation technique and observed superior performance of slit ribs in comparison to the full ribs. Hwang (1998) investigated the effect of slitted ribs on heat transfer in a rectangular channel using laser holographic interferometry and observed superior heat transfer performance of the slit-ribbed channel. Ekkad and Han (1997) presented the Nusselt number distributions in a two-pass square channel with one ribbed wall using transient liquid crystal thermography and showed the effect of the secondary flows induced by the 180^o turn. Mochizuki et al. (1999) investigated the heat transfer and fluid flow in two straight rectangular channels with a 180^o sharp bend and observed that the heat transfer characteristics downstream from the bend are controlled by secondary flows generated in the bend.

The role of secondary flow on manipulating the fluid flow and heat transfer in a ribbed duct is well established from the above literature survey. The present work proposes a new slit rib geometry (Fig. 1) with a continuous slit inside the rib. The motive behind the proposed rib geometry is to manipulate the reattaching shear layer from the top surface of the rib by means of the secondary flow coming out from the slit. It is expected that the large-scale vortices present in the reattaching shear layer will be manipulated by the vortices present in the secondary flow from the slit by vortex merging/pairing mechanism. The heat transfer enhancement due to the slit rib has been compared with that of the solid rib from using liquid crystal thermography. Thermodynamic performance evaluation based on entropy generation analysis (Bejan, 1996) is carried out to compare the performance of rib turbulators from both heat transfer augmentation and pressure penalty points of view.

2. Apparatus and Instrumentation

The sketch of the experimental setup with instrumentation used in this work is shown in Fig. 1. The experimental facility comprises of a flow circuit, an image processing system, the traverse mechanism and the heating section. The experiments are performed in an open-loop airflow system. The air is sucked into the test section through a honeycomb section, five anti-turbulence screens and a 3:1 contraction cone. The test section is followed by a flow straightener to minimize the influence of blower noise in the test section. The speed of the blower is controlled by a speed controller (Victor G1000, Kirloskar Electric). The test channel is 3300mm long with an aspect ratio of 1.8:1 (298mm×160mm in the vertical plane) and is made of Perspex sheet of 12 mm thickness. The free stream turbulence level at the entrance of the test cell is 0.5% for the velocity range used in this work.

A single aluminum plate (680mm× 298mm×3mm) heated by stainless steel foil from underneath acts as the heat transfer surface. Six stainless steel foils of dimension 680mm×47mm×0.045mm connected in series are adhered uniformly between the aluminum plate and 25mm thick bakelite sheet. A DC power source supplies power to the stainless steel foil heaters. To minimize the conductive heat losses, the lower surface of the bakelite sheet is insulated using a 13mm thick plate of bakelite with a 2mm air gap in between. The heat transfer surface is instrumented with thirteen calibrated thermocouples of the chromel-alumel type, along the centerline and spanwise direction of the heated Aluminum plate. Conduction losses to the bottom surface

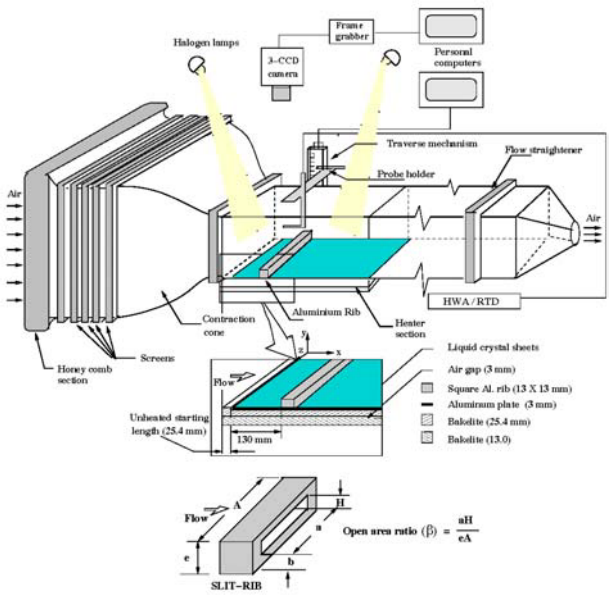

Fig. 1. Schematic diagram of flow system, coordinate system and instrumentation.

of the heating section are estimated by the thermocouples mounted onto the bakelite plate at several locations.

The temperature of the test surface was measured using K-type thermocouples connected to the National Instrument's data acquisition card (NI-4351) and liquid crystal thermography (LCT). The heating surface is coated with a thin layer of TLCs sheet (Hallcrest, R35C5W). The image acquisition and processing system used in the present investigation consists of a high resolution 768 (horizontal) × 574 (vertical) pixels 3-CCD video camera (SONY XC-003P) with 16mm focal length lens (VCL-16WM), a 24-bit colour frame grabber board (Imaging Technology) and a high speed PC. More details on the calibration of liquid crystals have been discussed by Tariq et al.(2003).

Errors in the experimental data are associated with measuring temperature by K-type thermocouples, fluctuating supply voltage of the dc power source, positional accuracy in locating the probe, errors in calibration data and inadequate compensation for room temperature, drift in electronics, non-uniformity in the illumination on the liquid crystals and the uniformity in the pixel quality of the liquid crystal sheets. Computer controlled traverse mechanism has been used for positioning having ±0.1mm positional accuracy. The room temperature is controlled within ±0.5°C and maintained uniform throughout the experiment. The liquid crystal measurements were repeated number of times and the data analysis was carried out for different time intervals between the transient images and also by increasing total time span of the transient run. The maximum uncertainty in the local heat transfer coefficient from LCT was observed to be 10%.

3. Data Analysis

3.1 Transient Liquid Crystal Thermography

An inverse transient approach is adopted for evaluating the heat transfer coefficient from the liquid crystal thermography. The test section is heated to a constant temperature and then subjected to step cooling by turning the heater off and flowing ambient air over it. The rate of cooling of the surface of the heated test section is recorded by monitoring the colour change patterns of the LC sheets with respect to time. The semi-infinite solid assumption has been verified from the transient temperature measurement of the thermocouples located on the top and bottom of the bakelite plate and the aluminum test surface. The bottom surface of the bakelite plate maintains constant temperature during the cooling period of the test surface indicating the validity of the infinite solid assumption. Solving the 1-D transient conduction equation with prescribed initial temperature, $T_{w,i}$ and boundary conditions (convective boundary condition at $t > 0$), one obtains the non-dimensional temperature at the convective boundary surface as (Ireland and Jones, 2000 and Ekkad and Han, 2000):

$$\frac{T_{w,i} - T_w(t)}{T_{w,i} - T_b} = 1 - \exp\left(\frac{h^2 \alpha t}{k^2}\right) erfc\left(\frac{h\sqrt{\alpha t}}{k}\right) \tag{1}$$

where, $T_w(t)$ is the surface temperature at time t, T_b is the bulk mean temperature, $T_{w,i}$ is the initial surface temperature, h is the convective heat transfer coefficient, α is the thermal diffusivity and k is the thermal conductivity of the bakelite plate. The transient non-dimensional temperature variation of the test surface is curve fitted using the above equation with the local heat transfer coefficient *(h)* as a parameter.

3.2 Performance Evaluation

The thermodynamic performance evaluation has been carried out by comparing the dimensionless augmentation numbers: the augmentation Nusselt number, $N_{\overline{Nu},a}(=\overline{Nu}_a/\overline{Nu}_o)$, the augmentation Nusselt-friction-factor number, $N_{\overline{Nu}\overline{f},a}(=(\overline{Nu}/\overline{f})_a/(\overline{Nu}/\overline{f})_o)$, the augmentation entropy generation number, $N_{S,a}(=\dot{S}'_a/\dot{S}'_o)$ and the irreversibility distribution ratio, $\phi(=\dot{S}'_{\Delta P}/\dot{S}'_{\Delta T})$, where $\dot{S}'$ is the entropy

generation rate per unit heated length. In these notations the subscript '*a*' refers to the augmented passage and the subscript '*o*' refers to the original (unaugmented) passage. The subscripts ΔP and ΔT represents the irreversibilities caused by fluid friction and heat transfer, respectively.

The irreversibility of convective heat transfer is primarily due to two effects: heat transfer across a finite (non-zero) temperature difference and fluid friction. The main objective of heat transfer augmentation is to increase the wall-fluid heat transfer coefficient without a substantial increase in the pumping power demanded by the forced convection arrangement. Thus, the true effect of a proposed augmentation technique on thermodynamic performance may be evaluated by comparing the irreversibility of the heat exchange arrangement before and after the implementation of the augmentation technique. Augmentation entropy-generation number, $N_{S,a}$ is useful in quantizing the thermodynamic impact of an augmentation technique. Augmentation techniques that are characterized by $N_{S,a}$, values of less than one are thermodynamically advantageous. Augmentation entropy-generation number is determined by computing $\dot{S}'$ for both the augmented and unaugmented passages (baseline case) using entropy generation rate formula (Bejan, (1996)).

$$\dot{S}' = \frac{\dot{m}}{\rho T^*}\left(-\frac{dP}{dx}\right) + \frac{q'\Delta T}{T^{*2}} \tag{2}$$

where T^*, ΔT and q' are the absolute bulk temperature of the inlet stream ($\dot{m}$), wall-bulk-fluid temperature difference averaged over heated length, L ($=\frac{1}{L}\int_0^L [T_w(x) - T_b(x)]dx$), and the heat transfer rate per unit heated length, respectively. The pressure gradient, $\frac{dP}{dx}$ is substituted by the average pressure gradient $\frac{\Delta P}{L}$ measured over the entire heated test section. First term on the right side of Equation 2 represents the fluid-flow irreversibility and the second term is the heat transfer irreversibility. The relative importance of the two-irreversibility mechanism is described by the irreversibility distribution ratio ϕ, which is defined by (Bejan, (1996)):

$$\phi = \frac{\text{fluid flow irreversibilty}}{\text{heat transfer irreversibilty}} = \frac{\frac{\dot{m}}{\rho T^*}\left(-\frac{\Delta P}{L}\right)}{q'\Delta T} T^{*2} \tag{3}$$

4. Results and Discussion

4.1 Energy Balance Check

To verify our experimental procedure and assumptions, a detailed energy balance check has been performed. In the first energy balance approach, the control volume was assumed to consist of the inflow-plane, the outflow-plane and the heated surface of the test section. The net heat transfer rate from the heated surface of the test section to the air (Q_{net}) is calculated as the difference in enthalpy ($\rho u\ c_p\ T$) between the inlet and outlet of the flow. The second energy balance check was carried out considering the test surface as the control volume. The heat loss (conduction and radiation) from the surface was subtracted from the total power input (voltage (V) × current (I)) to provide the net convective heat transfer (Q_{net}) from the test surface. A 1-D conduction model was used to compute the conduction heat losses to the bottom of the test section. The radiation losses were estimated for the heated plate using emissivity, ε = 0.92 for the liquid crystal sheet. The average conduction and radiation losses were observed to be about 8 to 24% of the total electrical power input respectively. The average convective heat transfer is presented in terms of the average Nusselt number, defined as:

$$\overline{Nu} = \frac{Q_{net} D_h}{k \frac{1}{L}\int_0^L [T_w(x) - T_b(x)]dx} \tag{4}$$

The average augmentation Nusselt number for the solid rib obtained from the LCT technique is compared with that obtained from the two-energy balance approaches in Table 1. The augmentation Nusselt number obtained from the two energy balance approaches are within 5% of each other. The small discrepancy between the two may be attributed to the inherent uncertainty in the experiment and data analysis. The difference between the augmentation Nusselt number obtained from LCT and energy balance approaches is in the range between 10% to 22%; the value obtained from LCT being consistently smaller than that of the energy balance approaches. The plausible explanation for the lower augmentation Nusselt number value from LCT compared to the energy balance approaches is attributed to the fact that the total dimension of the image used for LCT is less than the total area of the heated section limited by the field of view of the camera lens.

Table 1. The augmentation Nusselt number ($N_{\overline{Nu},a}$) for solid rib from LCT analysis and energy balance approach (electrical power input and flow enthalpy).

Re	$N_{\overline{Nu},a}$ (Solid rib)		
	Power-Input	Enthalpy	LCT
13400	1.39	1.43	1.28
22600	1.66	1.69	1.48
32100	1.61	1.60	1.40
40800	1.49	1.53	1.19

4.2 Nusselt Number

The applicability of the transient LCT in calculating the augmentation Nusselt number has been established by comparing the LCT results with the two energy balance approaches in the preceding section. A second validation has been carried out by comparing the spanwise averaged Nusselt number from LCT with that from the law of the wall by Tariq et al.(2003). The stream-wise variation of the local Nusselt number from the law of the wall compares well with that obtained from the transient LCT; the maximum deviation between the two being ≈ 8%, indicating the validity of the LCT approach for determining the heat transfer coefficient of turbulent flow.

The surface Nusselt number and the spanwise averaged Nusselt number for the solid rib and the slit rib are compared in Fig. 2. For the slit rib, different open area ratio (β) values i.e. 10%, 20%, 30%, 40% and 50% have been considered. The corresponding augmentation Nusselt number results are presented in Table 2. No significant variation of the Nusselt number in the spanwise direction is observed from the surface Nusselt number plot in Fig. 2. This indicates that the presence of the slit inside the rib has not contributed to any significant spanwise vortical structures and the overall two-dimensional character of the flow is maintained for both solid and slit rib. The slit ribs (β = 40% and β = 50%) are not effective for heat transfer augmentation in comparison to the solid rib at all Reynolds numbers. The slit rib (β = 30%) is more effective at *Re* = 22600 and 32100 but less effective at Re = 13400 and 40800 in comparison to the solid rib. The augmentation Nusselt numbers are highest for the slit ribs (β = 10% and β = 20%) at all Reynolds number (Table 2). The overall heat transfer of the slit rib (β = 20%) is marginally superior than the slit rib (β = 10%) at *Re* = 32100 and 40800.

The spanwise averaged Nusselt number plot shown in Fig. 2 shows that the slit ribs (β = 10% and β = 20%) are more effective than the solid rib in the far field region at all Reynolds numbers. The secondary flow coming out from the slit manipulates the reattaching shear layer in the downstream direction and is therefore responsible for the heat transfer effectiveness in the far field region. The surface Nusselt number plot at *Re* = 13400 and 22600 shows that the reattachment length of the slit rib (β = 10%) is less than the solid rib. The spanwise averaged Nusselt number in the near field region for the slit rib (β = 10%) is enhanced in comparison to the solid rib. But, no effect on heat

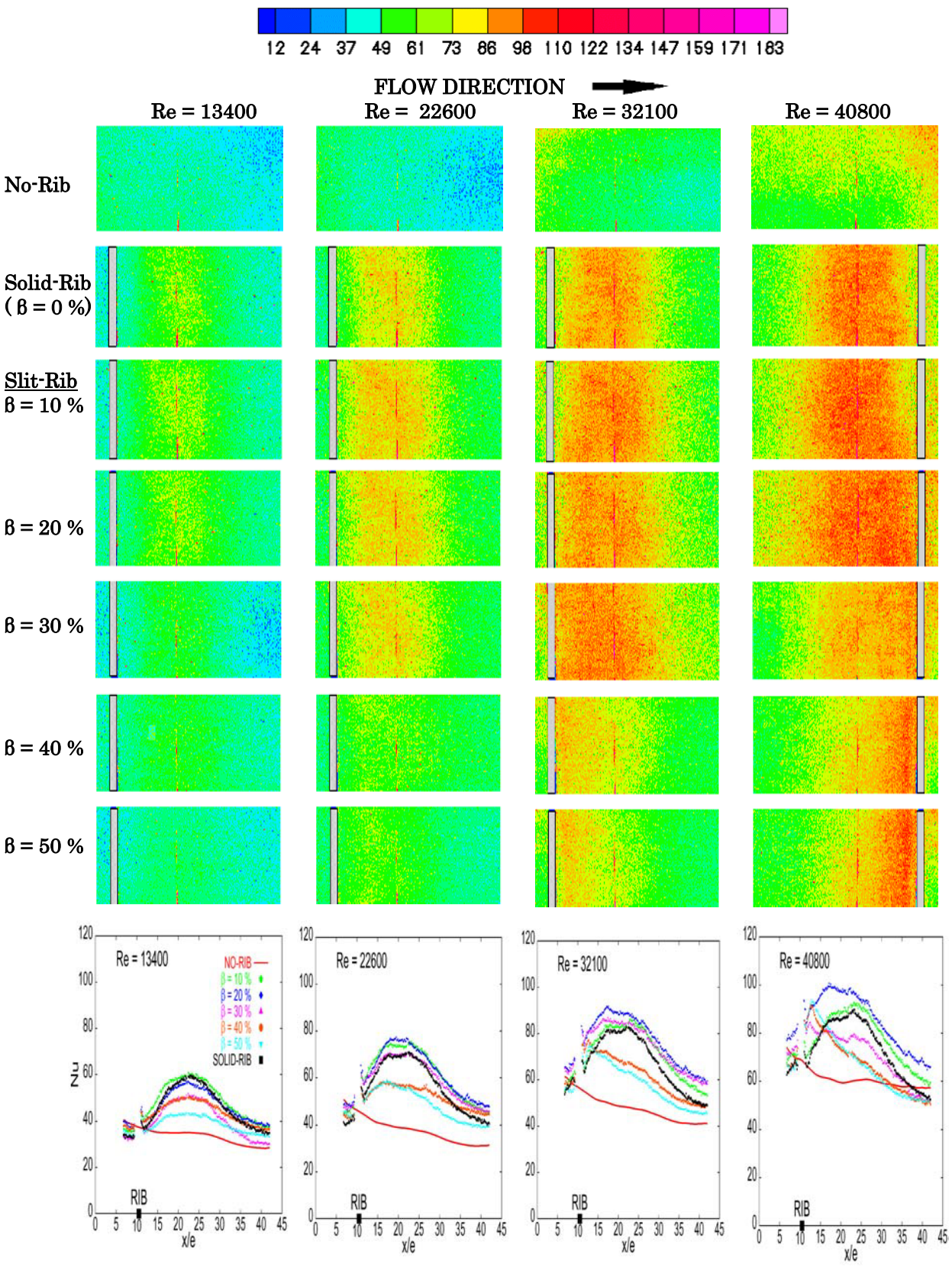

Fig. 2. The surface Nusselt number and span-wise averaged Nusselt number of solid rib and slit ribs (open area ratio, β = 10%, 20%, 30%, 40% & 50%) at different *Re*.

Table 2. The augmentation Nusselt number ($N_{\overline{Nu},a}$) comparison between solid rib and slit rib (with different open area ratios, β) at different Reynolds numbers.

Re	Augmentation Nusselt number ($N_{\overline{Nu},a}$)					
	Solid rib	Slit rib with open area ratio (β =)				
		10%	20%	30%	40%	50%
13400	1.28	1.35	1.36	1.13	1.21	1.08
22600	1.48	1.62	1.64	1.56	1.36	1.29
32100	1.40	1.49	1.61	1.55	1.29	1.22
40800	1.19	1.26	1.39	1.16	1.10	1.10

transfer in the near field region is observed for the slit rib (β = 10%) at higher Reynolds numbers (= 32100 and 40800). The surface Nusselt number distribution at *Re* = 32100 and 40800 shows that the recirculating region behind the solid rib is small in comparison to that at *Re* = 13400 and 22600. This may be the limiting factor on the influence of the secondary flow out of the slit on the heat transfer enhancement in the near field region at *Re* = 32100 and 40800.

The spanwise averaged Nusselt number distribution results in Fig. 2 show that at higher Reynolds numbers (= 32100 and 40800), the heat transfer in the near field region is higher than the solid rib for all open area ratio cases (β = 10%, 20%, 30%, 40% and 50%). For the lower open area ratio cases (β = 10% and 20%), the presence of the slit manipulates the reattaching shear layer as the heat transfer enhancement is significant both in the near field and far field region. While for the larger open area ratio cases (β = 30%, 40% and 50%) the lower portion of the slit rib acts like an independent solid rib with its own reattachment zone. Hence, the overall zone for heat transfer effectiveness is confined to the near field region only.

As the effectiveness of the slit in enhancing the heat transfer is established from the preceding discussion, one asks the question if the value of the open area ratio (β) is the only guiding factor or the location of the slit from the bottom surface of the channel (*b/e*) has any influence on the heat transfer enhancement. To investigate this, the location of the slit from the bottom of the test surface is varied as a parameter (*b/e* = 0.24, 0.29, 0.35, 0.40, 0.46, 0.52 and 0.57) for the slit rib (β = 20%). The slit rib (β = 20%) is selected due to its superior performance, which is discussed in the following section. The slit located at *b/e* = 0.40 corresponds to the symmetric location, i.e. the slit is located at the same distance from the top surface and the bottom surface. The lower *b/e* values are closer to the bottom surface and higher b/e values are away from the bottom test surface in comparison to the symmetric location. The surface Nusselt number and the spanwise averaged Nusselt numbers for different slit locations are presented in Fig. 5 and the corresponding augmentation Nusselt numbers are presented in Table 3. At *Re* = 13400 and 22600, the symmetrically located slit (*b/e* = 0.4) is the most effective in comparison to other slit locations (Table 3). At *Re* = 32100 and 40800, the slit location *b/e* = 0.35 is equally effective as *b/e* = 0.40 (Table 3). The surface Nusselt number distribution shown in Fig. 3 shows that the location of the slit does not influence the upstream recirculating region, and there is no systematic influence of the slit location on the heat transfer augmentation. Overall, the symmetric location of the slit is the optimum one from heat transfer enhancement point of view.

Table 3. The augmentation Nusselt number ($N_{\overline{Nu},a}$) for slit ribs (β = 20%) with different slit locations (*b/e*) from the bottom test surface at different Reynolds numbers.

Re	Augmentation Nusselt number ($N_{\overline{Nu},a}$)						
	b/e =0.24	*b/e*=0.29	*b/e*=0.35	*b/e*=0.40	*b/e*=0.46	*b/e*=0.52	*b/e*=0.57
13400	1.24	1.25	1.19	1.36	1.24	1.24	1.28
22600	1.48	1.59	1.54	1.64	1.51	1.58	1.55
32100	1.53	1.50	1.64	1.61	1.52	1.56	1.58
40800	1.44	1.37	1.44	1.39	1.33	1.38	1.40

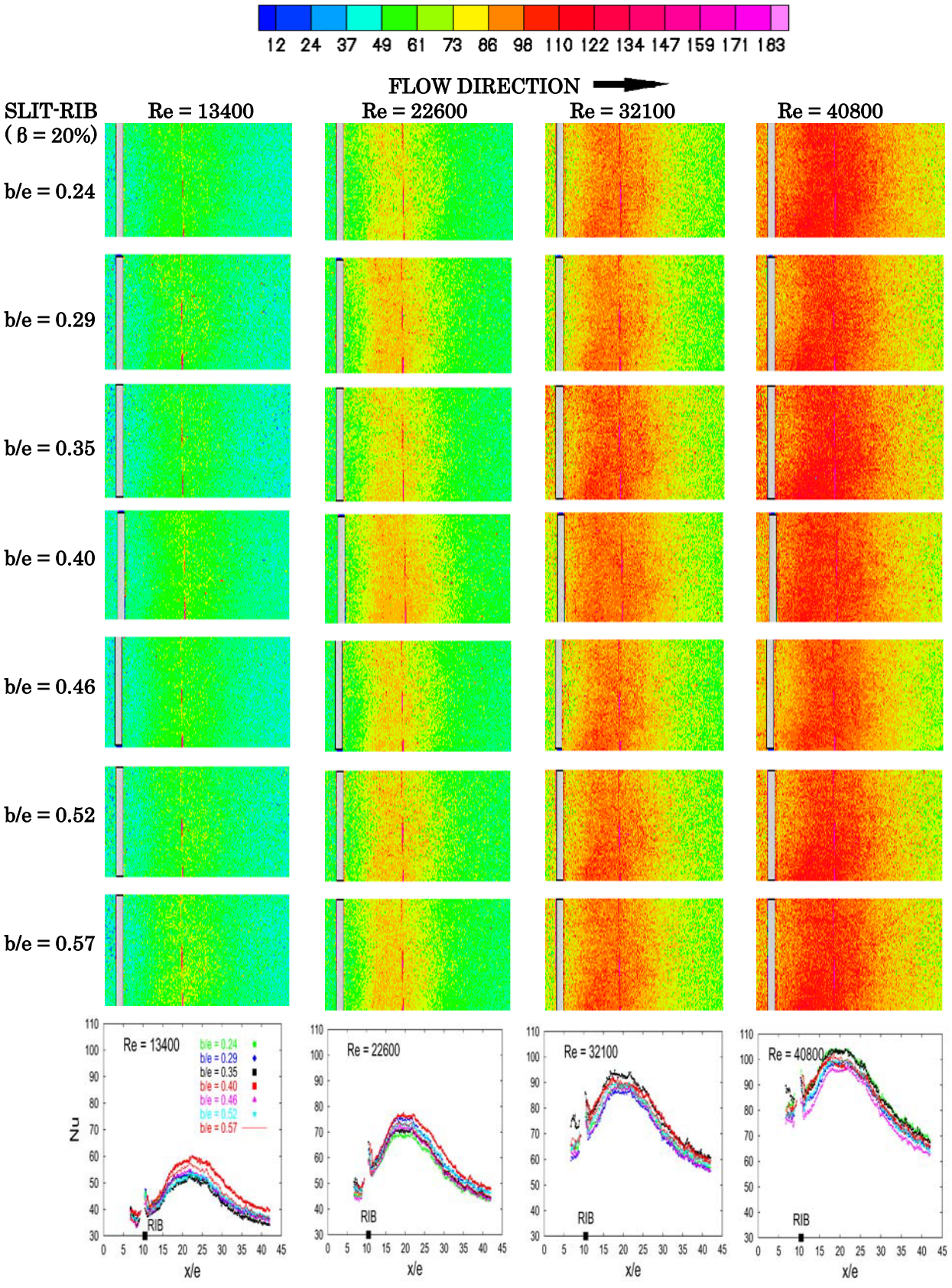

Fig. 3. The surface Nusselt number and span-wise averaged Nusselt number of the slit rib (β = 20%) for different slit positions from the bottom test surface (*b/e*) at different *Re*.

4.3 Performance Evaluation

We have observed in the preceding section that the slit location $b/e = 0.35$ and 0.40 for slit rib ($\beta = 20\%$) has similar heat transfer performance, the later location being marginally superior. While taking pressure penalty into account, the optimum b/e location conclusion may change. Therefore, the performance analysis results of the slit rib ($\beta = 20\%$, $b/e = 0.35$ and 0.40) based on entropy generation principle are compared with the solid rib in Table 4. The slit rib ($b/e = 0.40$) has higher heat transfer augmentation at all Reynolds number in comparison to the solid rib. The friction factor for the slit rib ($b/e = 0.40$) is smaller than the solid rib at all Reynolds number indicating reduced pressure penalty for the slit rib. The slit rib ($b/e = 0.35$) is more effective than the solid rib at higher Reynolds numbers, i.e. $Re = 32100$ and 40800 from heat transfer point of view. The corresponding friction factor for the slit rib is lower than the solid rib. Therefore, the slit rib geometry is observed to provide larger heat transfer augmentation and reduced pressure penalty in comparison to the solid rib.

The Nusselt friction factor number ($N_{\overline{Nu},\overline{f},a}$) shows the ratio of the Nusselt number increase to the friction factor increase due to the augmentation geometry. The Nusselt friction factor number ($N_{\overline{Nu},\overline{f},a}$) for the slit rib geometry is always higher than the solid rib indicating that the increase in heat transfer augmentation for the slit rib does not have a commensurate increase in pressure penalty (see Table 4). The entropy generation for the slit rib ($b/e = 0.40$) is lower than the solid rib at all Reynolds number confirming the observation made above based on heat transfer augmentation and friction factor. The largest drop in entropy generation (= 37%) is observed for the slit rib ($b/e = 0.40$) at $Re = 32100$ in comparison to 6% for the solid rib. There is 61% augmentation in Nusselt number for the slit rib ($b/e = 0.4$) in comparison to 40% for the solid rib. The slit rib ($b/e = 0.35$) has been observed earlier to be less effective than the solid rib from heat transfer augmentation point of view at $Re = 13400$ and 22600. But, the entropy generation number ($N_{S,a}$) (see Table 4) is lower at the corresponding Reynolds number for the slit rib ($b/e = 0.35$) in comparison to the solid rib indicating lower entropy generation for the slit rib compared to the solid rib. Thus, the slit rib is superior than the solid rib from both heat transfer and pressure penalty point of view at all Reynolds number considered. The irreversibility ratio (ϕ) for the smooth duct are 0.001,0.003, 0.005 and 0.0116 at Re = 13400, 22600, 32100 and 40800 indicating higher entropy generation due to the heat transfer than that due to the pressure drop. The irreversibility ratio for the solid rib and slit rib are higher than the smooth duct values (see Table 4) indicating the drop in entropy generation from heat transfer. The irreversibility ratio increases with increase in Reynolds number. But the increase in irreversibility ratio does not necessarily indicate the drop in total entropy generation, which is evident from the entropy generation number ($N_{S,a}$) results shown in Table 4; the entropy generation for slit rib is lowest at Re = 32100, and the irreversibility ratio is highest at $Re = 40800$. But, from thermodynamic point of view, the entropy generation is a true indicator for the performance comparison and thus best overall thermodynamic performance is achieved at $Re = 32100$ for the slit rib ($\beta = 20\%$).

Table 4. Performance evaluation parameters using entropy generation principle for solid rib and slit ribs (β = 20%; b/e = 0.35 and b/e = 0.40).

Rib type	Re	$\overline{Nu}$	$\overline{f}\times10^3$	$N_{\overline{Nu},\overline{f},a}$	$N_{\overline{Nu},a}$	$N_{S,a}$	$\phi\times10^3$
Solid rib	13400	45.69	45.550	0.802	1.28	1.13	1.6185
	22600	55.97	39.693	0.691	1.48	0.94	7.4155
	32100	67.05	35.508	0.460	1.40	0.94	20.224
	40800	72.86	34.472	0.271	1.19	0.87	63.002
Slit rib (β = 20%) with b/e = 0.35	13400	42.59	42.655	0.797	1.19	0.96	1.7984
	22600	58.08	39.557	0.724	1.54	0.92	7.6013
	32100	78.35	33.336	0.567	1.64	0.65	22.220
	40800	87.94	31.379	0.355	1.44	0.88	56.167
Slit rib (β=20%) with b/e = 0.40	13400	46.40	45.449	0.815	1.36	0.81	2.0631
	22600	62.06	37.550	0.814	1.64	0.79	9.0789
	32100	76.78	33.185	0.560	1.61	0.63	28.343
	40800	85.19	30.833	0.350	1.39	0.90	53.844

5. Conclusion

The effectiveness of the solid rib and the slit rib mounted on the bottom surface of a rectangular channel on heat transfer enhancement has been investigated experimentally. The liquid crystal thermography is used to visualize the surface Nusselt number distribution. The combined effect of heat transfer enhancement and pumping power penalty is analyzed using the entropy generation principle. The open area ratio of the slit rib, the location of the slit from the bottom surface and the Reynolds number are the parameters considered in the detailed analysis. The heat transfer augmentation for the slit rib is higher than that for the solid rib with reduced pressure penalty. The open area ratio of the slit rib plays an important role, with a 20% open area ratio being optimum. The symmetric location of the slit i.e. the slit located at same distance from the top and bottom of the rib is observed to be the optimum location. The slit rib (β = 20%) has 61% enhancement of heat transfer and 37% drop in entropy generation at Re = 32100 in comparison to the respective values of 40% and 6% for the solid rib. The presence of the slit does not contribute to three dimensionality of the flow, i.e. the Nusselt number distribution in the spanwise direction does not show the presence of any spanwise structures. The slit rib is superior to the solid rib from both heat transfer augmentation and pressure penalty points of view.

References

Acharya, S., Dutta, S. Myrum, T. A. and Baker, R. S., Periodically Developed Flow and Heat Transfer in a Ribbed Duct, Int. J. Heat Mass Transfer, 36 (1993), 2069-2082.

Bejan, A., Entropy Generation Minimization, (1996), 71, CRC Press.

Chyu, M. K. and Natarajan, V., Effects of a Slit in a Rib on the Heat Transfer from a Rib-mounted Wall, ASME J Heat Transfer, 115 (1993), 792-796

Ekkad, S. V. and Han, J. C., Detailed Heat Transfer Distributions in Two-pass Square Channels with Rib Turbulators, Int. J. Heat Mass Transfer, 40 (1997), 2525-2537.

Ekkad, S. V. and Han, J. C., A Transient Liquid Crystal Thermography Technique for Gas Turbine Heat Transfer Measurements, Meas. Sci. Technol., 11 (2000), 957-968.

Han, J. C. and Zhang, Y. M., High Performance Heat Transfer Ducts with Parallel Broken and V-shaped Broken Ribs, Int. J. Heat Mass Transfer, 35 (1992), 513-523.

Hwang, J. J., Heat Transfer-friction Characteristic Comparison in Rectangular Ducts with Slit and Solid Ribs Mounted on One wall, ASME J Heat Transfer, 120 (1998), 709-716.

Ireland, P. T. and Jones, T. V., Liquid Crystal Measurements of Heat Transfer and Surface Shear Stress, Meas. Sci. Technology, 11 (2000), 969-986.

Kukreja, R. T., Lau, S. C. and McMillin, R. D., Local Heat/mass Transfer Distribution in a Square Channel with Full and V-shaped Ribs, Int. J. Heat Mass Transfer, 36 (1993), 2013-2020.

Mochizuki, S., Murata, A., Shibata, R. and Yang, W. J., Detailed Measurement of Local Heat Transfer Coefficients in Turbulent Flow Through Smooth and Rib-roughened Serpentine Passages with a 180° Sharp Bend, Int. J Heat and Mass Transfer, 42 (1999), 1925-1934.

Schultz, D. L. and Jones, T. V., (1973) Heat Transfer Measurements in Short-duration Hypersonic Facilities, AGARD 165.

Tariq, A., Singh, K., and Panigrahi, P. K., Flow and heat transfer in a rectangular duct with single rib and two ribs mounted on the bottom surface, J. Enhanced Heat Transfer, 10(2) (2003), 171-198.

Author Profile

Pradipta Kumar Panigrahi: He received his B.S. (Honors) degree in Mechanical Engineering from UCE Burla, Orissa. He received his M.S. in Mechanical Engineering and Computer Science and his Ph.D. in Mechanical Engineering from Lousiana State University, Baton Rouge, USA. Currently he is working as an Assistant Professor in the Mechanical Engineering Department, IIT Kanpur, India. He visited JAPAN from January 2001 to July 2001 for a period of six months under BOYSCAST fellowship. His research interests are optical techniques, heat transfer enhancement, soft computing based modeling and control and turbulence.

Andallib Tariq: He received his B.E degree in Mechanical Engineering from Bangalore University and subsequently completed MBA from Bihar University. Further he studied in Mechanical Engineering and received his M.Tech from Indian Institute of Technology, Kanpur, India. He is currently pursuing Ph.D. at IIT Kanpur. His research interests are experimental fluid mechanics, turbulence, flow visualization and heat transfer enhancement.